ISSN (Print) : 0974-6846
ISSN (Online) : 0974-5645
Indian Journal of Science and Technology, *Vol 8(S8), 83–88, April 2015*
DOI: 10.17485/ijst/2015/v8iS8/64331

Clinical Decision Support System for Patients with Cardiopulmonary Function Using Image Processing

Hee-Joon Park[1*], Seok-Tae Seo[2] and Byung-Seop Song[3]

[1]Department of Biomedical Engineering, School of Medicine, Keimyung University, Daegu, Korea; hjpark@kmu.ac.kr
[2]Daegu-Gyeongbuk Medical Innovation Foundations, Daegu, Korea; kenneth78@dgmif.re.kr
[3]Department of Rehabilitation Engineering, School of Rehabilitation Science, Daegu University, Daegu, Korea; bssong@daegu.ac.kr

Abstract

Clinical decision support system for chest X-ray images was proposed in this paper, which is based on image processing and analysis methods to evaluate the normality of X-ray images. To segment lung regions from the chest X-ray images, threshold and morphological methods were applied. The feature selection and image measurement were performed to evaluate the normality of chest X-ray images. The results demonstrate that the segmentation results differ only marginally from the actual contours of lung regions and provide similar results with actual lung regions. Moreover, based on the measurement and feature selection, the interpretation of normality was facilitated, and the results of interpretation were similar with the diagnosis made by clinical experts.

Keywords: Chest X-Ray Diagnosis Support, Component, Image Measurement, Image Processing, Lung and Heart

1. Introduction

After the X-ray was discovered by Wilhelm Conrad Rontgen in 1895[1], this radiation has been widely using in diagnostic medicine. Various examination tools including Computed Tomography (CT) and Magnetic Resonance Imaging (MRI) have been developed and have supplanted the X-ray for some purposes. However, X-ray imaging is still the most common examination tool.

Despite the long history and popularity of X-ray technology, interpretation of X-ray images remains challenging due to image complexity and variation. Many studies have been undertaken to refine X-ray analysis. These include segmentation and enhancement[2–6], and detection of image abnormalities[2,7–10]. Especially, a variety of Clinical Decision Support Systems (CDSSs) or Computer-Aided Diagnosis (CAD) systems have been reported as aids to the clinical decision process[2,7,9,10]. Most of the proposed systems are limited to the detection of suspicious features from medical images. Moreover, the methods for lung region segmentation based on learning or landmarks, such as the those based on Active Shape Models (ASMs)[2–6], Neural Networks (NNs)[2,10], and knowledge[2] require an image-based experiential learning process. Despite the learning process, the methods all suffer from the difficulty in segmenting the lung region, which can display widely varying lung shape with a badly defined edge[11].

Even clinical experts are challenged to distinguish between normality or abnormality of lung field such as blood vessels and nodules[2]. Thus, a method which is robust and possible to support the clinical decision is needed. The present study proposes a support system to evaluate normality from chest X-ray images.

The proposed two-stage method consists of image segmentation to detect lung regions from chest X-ray images followed by measurement and texture analysis to evaluate normality of the given image. Using threshold and morphological processing, the lung regions are segmented from X-ray images. Moreover, measurement and texture analysis enables the distinction of normality and abnormality of cardiomegaly and lung.

*Author for correspondence

To show the effectiveness of the proposed method, we performed segmentation and measurement experiments on various chest X-ray images with diagnosis results by clinical experts, and compared the results between experimental results and the expert-derived diagnosis.

2. Materials and Methods

2.1 Object of Study

In this paper, 10 chest X-ray images, shown in Figure 1, were used. The diagnosis results according to images are summarized in Table 1.

2.2 Lung Region Segmentation

In this study, threshold and morphological methods-based segmentation were performed. The threshold value was selected using entropy maximization on smoothed histogram[12–17]. The segmentation algorithm is summarized as follows:

Step 1. Obtain histogram of input image and smoothen histogram using Gaussian kernel[14–16].

$$H^p(g) = \frac{1}{n}\sum_{z=0}^{L-1} h(z)\left[\exp\left(-\|g-z\|^2/\beta\right)\right]^p \qquad (1)$$

where, g and z represent gray levels [0, L – 1], n is the total number of pixels of image, and $h(z)$ is occurrence frequency of the gray level z. Moreover, the normalization parameter β is set as the variance, and smoothing parameter p is obtained by correlation comparison between H^p and H^{p+1} [13–15]. That is, the optimal parameter p is selected using Eq. (2).

(a) Image 1 (b) Image 2 (c) Image 3 (d) Image 4 (e) Image 5

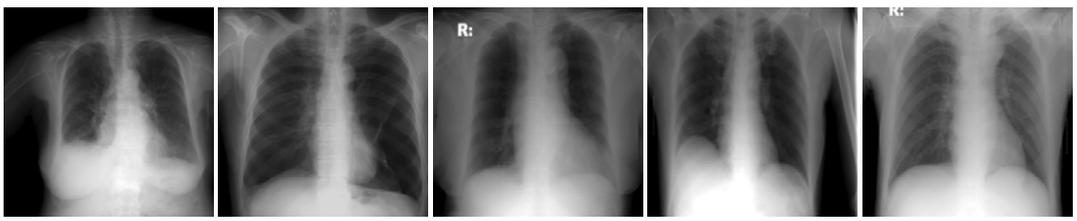

(f) Image 6 (g) Image 7 (h) Image 8 (i) Image 9 (j) Image 10

Figure 1. Chest X-ray images used in the study.

Table 1. Diagnosis results of the images

Image	Categories				
	Cardiomegaly	Pleural Effusion	Emphysematous	Pneumothorax	Overall Opinion
1	Severe				Abnormal
2					Normal
3			Yes		Abnormal
4	Mild	Both			Abnormal
5	Mild				Abnormal
6	Mild	Both			Abnormal
7				Left	Abnormal
8	Moderate				Abnormal
9					Abnormal
10					Normal

$$\left(1-cor^{p}\right)\le \varepsilon \tag{2}$$

where, cor^{p} denotes the correlation between H^{p} and H^{p+1}, and ε is an error criterion and we set ε as 10^{-4}.

Step 2. Based on smoothed histogram, the threshold value is selected by entropy maximization method[13,16]. When the probabilities of the partitions have the same value, entropy is maximized. Therefore the optimal threshold value is selected by Eq. (3).

$$T^{*}=\min\left(\sum\left|P_r\left(A_j\right)-\frac{1}{c}\right|\right),\ c=2,\ j=1,2 \tag{3}$$

where, A_j denotes j^{th} partition, which consists of gray levels $\left[T_{j-1}+1,T_j\right]$, $T_0=-1$.

Step 3. Perform dilation and erosion morphological processing with an adaptive mask[12,17].

Step 4. Detect lung region. An example of a segmentation is shown in Figure 2.

2.3 Image Measurement and Texture Analysis for the Diagnosis Support System

To evaluate the cardiomegaly and overall normality of chest X-ray image, size measurement and texture analysis methods[18–20] were applied. To evaluate cardiomegaly, the Cardiothoracic Ratio (CTR) was used. The features of lung region and example of CTR measurement based on the features are shown in Figure 3.

(a) Original image (b) Segmented (c) Region detection

Figure 2. Example of image segmentation.

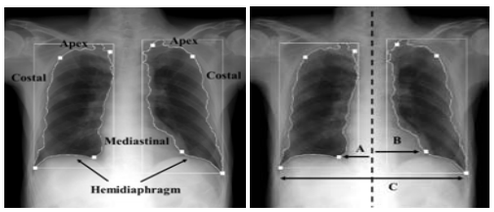

(a) Feature points (b) Cardiomegaly ratio

Figure 3. Feature points selection and CTR measurement in a chest X-ray image.

From the image in 4b, the CTR is defined as follows.

$$CTR=\frac{\left(A+B\right)}{C} \tag{4}$$

where, $(A + B)$ represents the transverse cardiac diameter and C represents transverse thoracic diameter.

In general, if the CTR is around 0.5, then the size of heart is normal. However, in an image measurement system, there could be an error between actual contour and computed contour of lung regions. Therefore, we applied another evaluation method to detect cardiomegaly, in which we evaluated cardiomegaly based not only on CTR but also on the ratio of pixel density of lung regions as follows:

Step 1. Project each lung regions according to the x-axis and y-axis.

Step 2. To divide segmented lung contour into apex, costal, hemi-diaphragm, and mediastinal part, compute the angle between projected axis and the candidate points.

Step 3. Select the points which have maximum distance from mid line of the thoracic spine.

Step 4. Using Eq. (5), compute CTR and lung regions pixel density ratio.

$$HR=\frac{\left(A+B\right)}{C}\times\frac{RD}{LD} \tag{5}$$

where, RD and LD represent the right lung pixel density and left lung pixel density, respectively.

Step 5. A HR >1.5 is diagnostic of cardiomegaly.

The reason for the use of the pixel density ratio of the right and left lung is to compensate for the error of segmentation regions from actual lung regions. Moreover, to evaluate the overall normality of lung from a chest X-ray image, the co-occurrence texture analysis method is applied.

Co-occurrence matrix is a statistical approach to analyze texture. The co-occurrence matrix used in this study was defined to four directions (0°, 45°, 90° and 135°) at distance 1. The co-occurrence matrix of given image is determined by using Eq. (6), and the normalized co-occurrence matrix p_{ij} is obtained using Eq. (7). The example of co-occurrence matrix is shown in Figure 4.

$$C_{ij}=\sum_{x=1}^{N}\sum_{y=1}^{M}\sum_{(a,b)\in S}\begin{cases}1, \text{ if } I(x,y)=i \text{ and } I(x,y)=j\\ 0, \text{ otherwise}\end{cases} \tag{6}$$

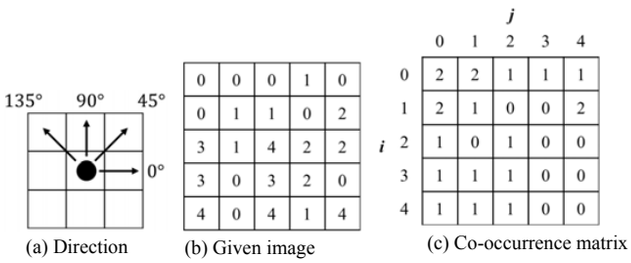

Figure 4. Example of co-occurrence matrix at direction 0° and distance 1.

$$p_{ij} = \frac{C_{ij}}{\sum_{i=0}^{L-1}\sum_{j=0}^{L-1} C_{ij}}, \sum_{i=0}^{L-1}\sum_{j=0}^{L-1} p_{ij} = 1 \tag{7}$$

where $I(x, y)$ denotes the gray level of image of size $M \times N$ at coordinate (x, y), S is a set of coordinates of direction (0°, 45°, 90° and 135°) with distance 1 at the center (x, y), and i, j represent the gray levels $[0, L-1]$.

From the co-occurrence matrix, ten Haralick texture descriptors (Entropy, Energy, Contrast, Homogeneity, Sum Average, Variance, Correlation, Maximum Probability, Inverse Difference Moment, and Cluster Tendency)[19,20] are computed to analyze the lung texture.

where, u_r, u_c, σ_r^2, σ_c^2 are the mean and variance of row and column of co-occurrence matrix, and are defined as follows:

$$u_r = \sum_{i=0}^{L-1}\sum_{j=0}^{L-1} i p_{ij},\ u_c = \sum_{i=0}^{L-1}\sum_{j=0}^{L-1} j p_{ij}$$
$$\sigma_r^2 = \sum_{i=0}^{L-1}\sum_{j=0}^{L-1} (i-u_r)^2 p_{ij},\ \sigma_c^2 = \sum_{i=0}^{L-1}\sum_{j=0}^{L-1} (i-u_c)^2 p_{ij} \tag{8}$$

Based on the computed Haralick features, we evaluated the normality between the right lung and left lung using cluster tendency. A marked difference between cluster tendencies of the lungs is indicative of differing lung characteristics, which could indicate a lung problem. Therefore, we evaluated the difference ratio from Eq. (9)

$$DCR = \frac{CL}{CR} \tag{9}$$

where, CR and CL represent the cluster tendency of the right lung and left lung, respectively. If the ratio is out of the range 1.0 ± 0.2, the chest X-ray image of the lung is judged abnormal.

Table 2. Haralick features and characteristics

Features	Description	Equation
Entropy	Measures the randomness of gray-level distribution	$-\sum_{i=0}^{L-1}\sum_{j=0}^{L-1} p_{ij} \log p_{ij}$
Energy	Measures the occurrence of repeated pairs within an image	$\sum_{i=0}^{L-1}\sum_{j=0}^{L-1} p_{ij}^2$
Contrast	Measures the local contrast in an image	$\sum_{i=0}^{L-1}\sum_{j=0}^{L-1} (i-j)^2 p_{ij}$
Homogeneity	Measures the homogeneity of an image	$\sum_{i=0}^{L-1}\sum_{j=0}^{L-1} \frac{p_{ij}}{\lvert i-j\rvert}, i \neq j$
Sum Average	Measures the average of the gray-level within an image	$\frac{1}{2}\sum_{i=0}^{L-1}\sum_{j=0}^{L-1} (i p_{ij} + j p_{ij})$
Variance	Measures the variation of gray level distribution	$\frac{1}{2}\sum_{i=0}^{L-1}\sum_{j=0}^{L-1}\{(i-u_r)^2 p_{ij} + (i-u_c)^2 p_{ij}\}$
Correlation	Measures a correlation of pixel pairs on gray-levels	$\sum_{i=0}^{L-1}\sum_{j=0}^{L-1} \frac{(i-u_r)(i-u_c) p_{ij}}{\sqrt{\sigma_r^2 + \sigma_c^2}}$
Maximum Probability (MP)	Determines the most predominant pixel pair in an image	$\max_{i,j} p_{ij}$
Inverse Difference Moment (IDM)	Measures the smoothness of an image	$\sum_{i=0}^{L-1}\sum_{j=0}^{L-1} \frac{p_{ij}}{1+(i+j)^2}$
Cluster Tendency (CT)	Measures the grouping of pixels that have similar gray-level values	$\sum_{i=0}^{L-1}\sum_{j=0}^{L-1} (i-u_r+j-u_c)^2 p_{ij}$

3. Experimental Results

To show the effectiveness of the proposed method, we applied it to 10 chest X-ray images with various characteristics (Figure 1). Some of the segmentation results are shown in Figure 5, and the parameter used in segmentation stage and the measurement results are summarized in Tables 3 and 4, respectively.

(a) Results of Image 4

(b) Results of Image 7

Figure 5. Segmentation results.

Table 3. The results according to image

Image	Kernel Parameter	Threshold Value	Mask Size	
			Dilation	Erosion
1	11	80	(10,10)	(20,20)
2	17	102	(10,10)	(20,20)
3	7	89	(10,10)	(20,20)
4	12	72	(10,10)	(20,20)
5	9	72	(10,10)	(10,10)
6	21	84	(3,3)	(20,20)
7	11	80	(5,5)	(10,10)
8	10	83	(5,5)	(20,20)
9	12	88	(10,10)	(20,20)
10	10	124	(5,5)	(20,20)

Table 4. Measurement results of images

Image	Measurement Index					
	CTR	Texture (Cluster Tendency)		Density of Pixel		HR
		Left	Right	Left	Right	
1	0.51646	543.6324	381.5131	153481	200516	1.3065
2	0.41485	1551.4931	1540.8273	373901	399065	1.0673
3	0.55197	1662.8031	648.8145	396019	333568	0.8423
4	0.52991	339.7002	339.2017	194694	238630	1.2257
5	0.51229	760.3008	756.9615	243040	356580	1.4672
6	0.53996	602.4436	602.8071	221340	217191	0.9813
7	0.44437	964.4407	613.8668	566767	521136	0.9195
8	0.47392	945.9067	946.1484	227079	297715	1.3111
9	0.40975	1158.7748	1122.5140	367427	349420	0.9510
10	0.46810	1527.2494	1183.2860	320622	439754	1.3716

Figure 5 and Table 3 show the segmentation results and the parameter values according to images. Figure 5a and 5b exemplifies the similarity of the different detected contours of lung regions by the proposed method with the difference from the actual contours of the lung regions. Although the proposed method does not always provide the best segmentation results, the similarity with the actual contours is compelling. Based on the segmented images, measurement and interpretation can be performed.

Table 4 shows the measurement results of CTR, texture, and lung ratio. Based on the measurement results, the interpretation was performed; the results are summarized in Table 5.

While the data from Tables 5 and 6 indicate that the proposed method provides accurate results for most, but not all, all cases of X-ray images. In particular, for Images 9 and 10, the proposed method did not provide accurate results, because of the difference between segmented contour and actual contour. Further improvement of segmentation accuracy for chest X-ray images is required

4. Conclusion

The chest X-ray is the most common and widely-used examination method in medicine. A plethora of studies

Table 5. Interpretation results

Image	Interpretation Results		Actual Diagnosis Results	
	Cardiomegaly	Overall Normality	Cardiomegaly	Overall Normality
1	Abnormal	Abnormal	Severe	Abnormal
2	Normal	Normal	Normal	Normal
3	Normal	Abnormal	Normal	Abnormal
4	Abnormal	Abnormal	Mild	Abnormal
5	Abnormal	Abnormal	Mild	Abnormal
6	Abnormal	Abnormal	Mild	Abnormal
7	Normal	Abnormal	Normal	Abnormal
8	Abnormal	Abnormal	Moderate	Abnormal
9	Normal	Normal	Normal	Abnormal
10	Abnormal	Abnormal	Normal	Normal

Table 6. Classification analysis results

	Accuracy	Sensitivity	Specificity
Cardiomegaly	0.9	0.8	1
Overall Normality	0.8	0.5	0.875

have been directed at improving the analysis of X-ray images; the approaches have included segmentation, edge detection, and nodule detection. However, analyzing an X-ray image in a CDSS remains several challenges. In this study, we propose a chest X-ray diagnosis support system based on image processing. We segmented lung regions of a given image based on threshold and morphological methods. Moreover, feature selection and image measurement were performed to evaluate the normality of chest X-ray images.

The results demonstrate that the segmentation results differ only marginally from the actual contours of lung regions and provide similar results with actual lung regions. Moreover, based on the measurement and feature selection, the interpretation of normality is facilitated, and the results of interpretation were similar with the diagnosis made by clinical experts.

However, we manually adopted a morphological mask size for dilation and erosion, and only cardiomegaly and normality were evaluated based on the proposed image measurement and feature selection. A segmentation method for chest X-ray images with more non-standard and complicated shape is needed, as are methods to evaluate more diseases such as pulmonary, pleural effusion, and pneumothorax diseases.

5. Acknowledgement

This research was supported by the MOTIE (Ministry of Trade, Industry and Energy), Korea, under the Inter-Economic Regional Cooperation program (R0002625) supervised by the KIAT (Korea Institute for Advancement of Technology).

6. References

1. Rontgen W. Uber eine neue art von strahlen. Sitzungsberichte der Physikalisch-Medicinisch Gesellschaftzu. Wurzburg; 1895. p. 132–41.
2. Ginneken BV, Romeny BMTH, Viergever A. Computer-aided diagnosis in chest radiography: A Survey. IEEE Trans Med Imag. 2001; 20(12):1228–41.
3. Yoshida H. Local contralateral subtraction based on simultaneous segmentation and registration method for computerized detection of pulmonary nodules. Proceedings of SPIE - The International Society for Optical Engineering; 2001. p. 426–30.
4. Li Q, Katsuragawa S, Doi K. Improved contralateral subtraction images by use of elastic matching technique. Med Phys. 2000; 27(8):1934–42.
5. Shi Y, Qi F, Xue Z, Chen L, Ito K, Matsuo H, Shen D. Segmenting lung fields in serial chest radiographs using both population-based and patient-specific shape statistics. IEEE Trans Med Imag. 2008; 27(4):481–94.
6. Silva JS, Silva A, Santos BS. Lung segmentation methods in X-ray CT images. Proceedings of SIARP 2000 5th Ibero-American Symposium on Pattern Recognition; 2000. p. 583–98.
7. Schilham AMR, Ginneken BV, Loog M. A computer-aided diagnosis system for detection of lung nodules in hest radiographs with an evaluation on a public database. Med Image Anal. 2006; 10:247–58.
8. Armato S, Giger M, MacMahon H. Computerized delineation and analysis of costophrenic angles in digital chest radiographs. Academic Radiol. 1998; 5:329–35.
9. Carreira M, Cabello D, Penedo M, Mosquera A. Computer-aided diagnoses:automatic detection of lung nodules. Med Phys. 1998; 25(10):1998–2006.
10. Coppini G, Diciotti S, Falchini M, Villari N, Valli G. Neural networks for computer-aided diagnosis: detection of lung nodules in chest radiograms. IEEE Trans Inform Tech Biomed. 2003; 7:344–57.
11. Klim S, Mortensen S, Bodvarsson B, Hyldstrup L, Thodberg HH. More active shape model, image and vision computing, NZ; 2003. p. 396–401.
12. Gonzalez RC, Woods RE. Digital Image Processing. 2nd ed. NJ: Prentice Hall; 2002.
13. Cao L, Shi ZK, Cheng EKW. Fast automatic multilevel thresholding method. Electron Lett. 2002; 38(16):868–70.
14. Wu KL, Yang MS. Mean shift-based clustering. Pattern Recogn. 2007; 40(11):3035–52.
15. Scholkopf B, Smola AJ. Learning with kernels: support vector machines, regularization, optimization, and beyond. UK: MIT Press; 2001.
16. Seo ST, Lee IK, Jeong HC, Kwon SH. Gaussian kernel-based multi-histogram equalization. IEICE Trans Info Syst. 2010; E39-D(5):1313–6.
17. Giardina CR, Dougherty ER. Morphological methods in image and signal processing. NJ: Prentice Hall; 1988.
18. Susomboon R, Raicu D, Furst J, Johnson TB. A co-occurrence texture semi-invariance to direction, distance and patient size. Proceedings of SPIE Medical Imaging. 2008; 6914(2):69141Y1-6.
19. Petrou M, Sevilla PG. Image Processing: Dealing with Texture. Wiley; 2006.
20. Susomboon R, Raicu DS, Furst J. Pixel-based texture classification of tissues in computed tomography. CTI Research Symposium; 2006.